Laminated bamboo lumber (LBL) in compression perpendicular to the grain direction: Experimental investigation and finite element analysis

Chaokun Hong[1], Haitao Li[2*], Dong Yang[3], Xin Li[4], Rodolfo Lorenzo[5], Mahmud Ashraf[6]

[1] PhD Candidate, College of Civil Engineering, Nanjing Forestry University, Nanjing 210037, China; Joint International Research Laboratory of Bio−composite Building Materials and Structures, Nanjing Forestry University, Nanjing 210037, China; College of Civil Engineering and Architecture, Zhejiang University, Hangzhou 310058, China. Email: hck@zju.edu.cn

[2*] Professor, College of Civil Engineering, Nanjing Forestry University, Nanjing 210037, China; Joint International Research Laboratory of Bio−composite Building Materials and Structures, Nanjing Forestry University, Nanjing 210037, China (corresponding author). Email: lhaitao1982@126.com

[3] PhD Candidate, College of Civil Engineering, Nanjing Forestry University, Nanjing 210037, China; Joint International Research Laboratory of Bio−composite Building Materials and Structures, Nanjing Forestry University, Nanjing 210037, China. Email: dong_yang@njfu.edu.cn

[4] PhD Candidate, School of Engineering, Deakin University, Geelong Waurn Ponds, VIC 3216, Australia. Email: xinli@deakin.edu.au

[5] Lecturer, University College London, London WC1E 6BT, UK. Email: r.lorenzo@ucl.ac.uk

[6] Professor, School of Engineering, Deakin University, Geelong Waurn Ponds, VIC 3216, Australia. Email: mahmud.ashraf@deakin.edu.au

Abstract: Localized damage may occur due to the fact that laminated bamboo lumber (LBL) has a lower compressive strength perpendicular to the grain direction than it does parallel to the grain. In this study, the transverse compressive performance of LBL under entire-surface compression and local-surface compression is investigated. Load-displacement curves, stress-strain relationship, detailed failure modes and basic mechanical properties are obtained. The results show that despite the compressive strength and elastic modulus are nearly same in the two transverse orientations, the failure patterns are distinct due to the layer structure. Ramberg-Osgood relation is utilized to fit the stress-strain curves. Proportional limit strength are determined indicating that specimens compressed locally have a greater load bearing capability. Based on finite element analysis and theoretical study, the mechanism of the enhancement in proportional limit strength is revealed. Equations for determining the bearing load of a specimen under local compression in the elastic stage are

derived from the simulation data and logit model, considering the contact length and geometric size of the specimen. Additionally, parametric tests are conducted to determine the effect of bearing shape, bearing area, and loading mode on the stress distribution and bearing capacity.

Keywords: Laminated bamboo lumber; transverse compression; local compression; finite element analysis

1. Introduction

The use of bamboo for manufacturing engineering structures (Ghavami 2005; Li et al. 2019b; Liu et al. 2022; Lv et al. 2019; Méndez Quintero et al. 2022; Mimendi et al. 2022) and composite materials (Dixon et al. 2016, 2017; Qiu and Fan 2020) has attracted extensive attention from researchers, as the concepts of sustainable development and carbon neutrality continue to gain favor. From macro to micro scale, the light weight and good mechanical properties of raw bamboo materials and bamboo fiber reinforced composite materials have been successfully demonstrated (Dixon 2017; Dixon et al. 2015; Sharma et al. 2015; Song et al. 2017). Dixon et al. (Dixon 2017) placed bamboo in the broader context of cellular solids, investigated the structures and mechanical properties of dry bamboo tissue, and found the relations between density and mechanical properties. Although they found that natural bamboo at the same density of densified bamboo has higher properties, raw bamboo materials sometimes cannot fully meet the requirements for building materials due to their discontinuous mechanical properties and weak connections (Hong et al. 2019, 2020). Laminated bamboo lumber (LBL) is a common engineered bamboo material made by gluing together thin and flat bamboo laminates with a specified width and thickness (Li et al. 2013). It is lightweight, has significantly more stable physical and mechanical qualities, and has a uniform cross section (Dauletbek et al. 2021). Numerous experimental studies on LBL in parallel to the grain direction have been undertaken in recent years, including compressive and tensile strength (Wang et al. 2021b; Zhang et al. 2021), bending properties (Li et al. 2019a; Sinha et al. 2014), constitutive model (Chen et al. 2020; Wei et al. 2020), and axial and eccentric compression behavior of LBL columns (Hong et al. 2021b; a; Wang et al. 2021a). However, because the

material is anisotropic, the compressive strength is significantly lower in off-axis orientations, particularly perpendicular to the grain direction (Yang et al. 2020).

Similar to timber structures (Li et al. 2021; Sun et al. 2021; Wang et al. 2019), nearly all engineered bamboo constructions exist the condition of transverse compression during service. The simplest engineering example may be the overlapping area of main and secondary beams; traditional timber connections such as mortise-tenon joints can also occur transverse compression (Zhou et al. 2021). Madsen et al. (Madsen et al. 1982) considered the effect of specific geometry, and proposed a design method for wood subjected to stresses perpendicular to the grain. Based on the equilibrium method of plasticity, Van der Put (Van der Put 2008) studied the theoretical explanation of the bearing strength of locally loaded timber blocks. Leijten et al. (Leijten 2016; Leijten et al. 2012) investigated the evaluation of the strength predictive ability of three bearing models having an empirical, semiempirical or physical background. Numerous studies have been conducted on this topic in relation to timber constructions. Nevertheless, discussions on the models for the local bearing capacity perpendicular to the grain, and the necessity for designing compression stresses perpendicular to the grain against ultimate limit state (ULS) rather than against serviceability limit state (SLS) are still continuing (Brandner 2018), much less to LBL with no test standard or design code. Until yet, only a few investigations have been conducted on the transverse compression properties of laminated bamboo lumber. Yang et al. (Yang et al. 2020) investigated the off-axis compressive properties of LBL and discovered that the compressive strength is lowest perpendicular to the grain direction, while transverse compression failure mechanisms are absent. Tinkler-Davies et al. (Tinkler-Davies and Shah 2021) used digital image correlation (DIC) to explore the failure mechanism of LBL under transverse compression. However, the specimen's dimensions are 10 mm×21 mm×19 mm, which does not reflect the specimen's true compressive strength. The specimens studied in the preceding two studies are in the radial direction, omitting the specimen in the tangential direction. Besides, there is no research on the local compression behavior of LBL.

Although there are many laminated bamboo lumber constructions (Su et al. 2021), there is still a dearth of research on the mechanical behavior of LBL in transverse directions, particularly under local compression situations. Because laminated bamboo lumber (LBL) has a substantially lower compressive strength in perpendicular to the grain direction than it does in parallel to the grain direction, perpendicular-to-grain should be avoided in the design of bamboo construction. However, due to usage and aesthetic needs, the utilization of perpendicular-to-grain may be unavoidable and result in localized damage. Therefore, it is necessary to study this topic for promoting application of engineered bamboo. The compressive behavior of LBL in the two transverse directions is investigated in this paper using both experimental and numerical methods. The main objectives of this work are to evaluate the basic mechanical properties, identify failure patterns, and uncover failure processes. Finite element analysis is performed to help understand the reason for proportional limit strength increasing and stress distribution under local surface compression. On the basis of simulation results, equations for calculating the bearing load of specimen under local compression are established. In addition, the investigations are extended using the finite element method to explore the effect of bearing shape, bearing area, and loading mode on the stress distribution and bearing capacity of specimens subjected to local compression. The findings of this study can be used to develop realistic guidelines for designing LBL structures.

2. Methodology

2.1 Materials

All specimens used in current study were manufactured by Ganzhou Sentai Bamboo Company LTD., Ganzhou, China. They used Moso bamboo (from Yongan, Fujian, China) as raw material and resorcinol as adhesive to produce Laminated bamboo lumber (LBL); the production procedures started from the arrangement of bamboo laminates as shown in Figure 1 followed by the hot pressure technique implementing the pressure of 9 MPa for upper and lower surfaces and 6.5 MPa for left and right surfaces in 157 ℃ condition

for about 15 minutes to form components. It is worth noting that, to meet the requirements of specimen length, basic bamboo laminates were mechanical connected along the parallel-to-grain direction prior to pressure.

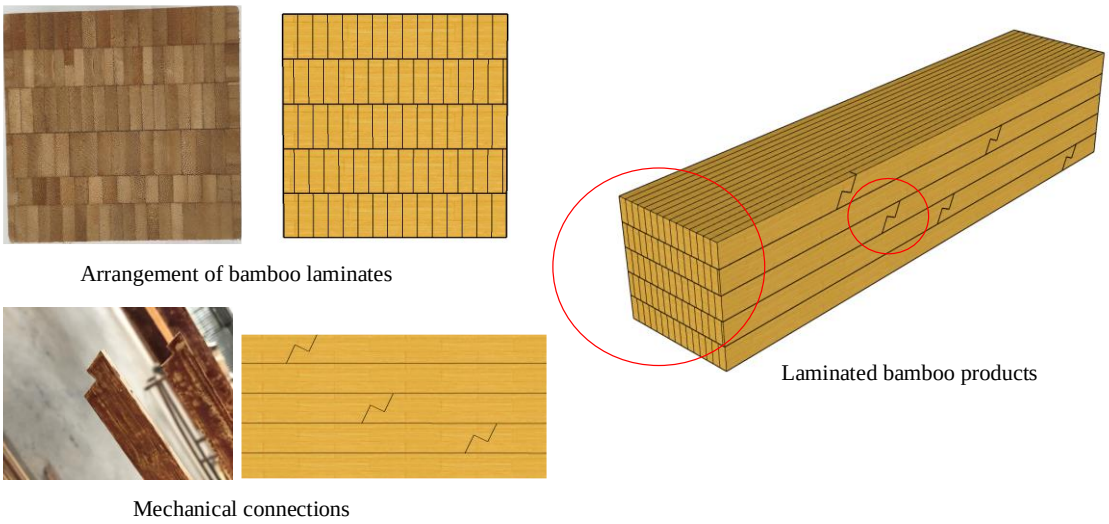

Figure 1 Arrangement of bamboo laminates and mechanical connection

2.2 Design of specimens

A total of 4 specimen groups including entire-surface compression specimens and local-surface compression specimens were prepared to investigate the transverse compressive behavior of laminated bamboo, as shown in Table 1 and Figure 2. CHH and CHV represent specimen under entire-surface compression in the radial direction and tangential direction respectively. PH and PV represent specimen under local-surface compression in the radial and tangential direction. Dimensions for specimens subjected to entire-surface compression were designed as 50 mm×50 mm×100mm, while that for partial compressive specimens were 50mm×50mm×150mm. The wide surface of bamboo strip was marked as ‘A’ followed by ‘B’, ‘C’ and ‘D’ marked successively along the counter clockwise direction in all specimens. ‘*’ was then used to mark top surfaces, whilst left bottom surfaces blank.

Table 1 Details of test specimens

Group	Dimension	Number	Compression direction
CHH	50mm×50mm×100mm	36	Radial direction
CHV		36	Tangential direction

PH	50mm×50mm×150mm	36	Radial direction
PV		36	Tangential direction

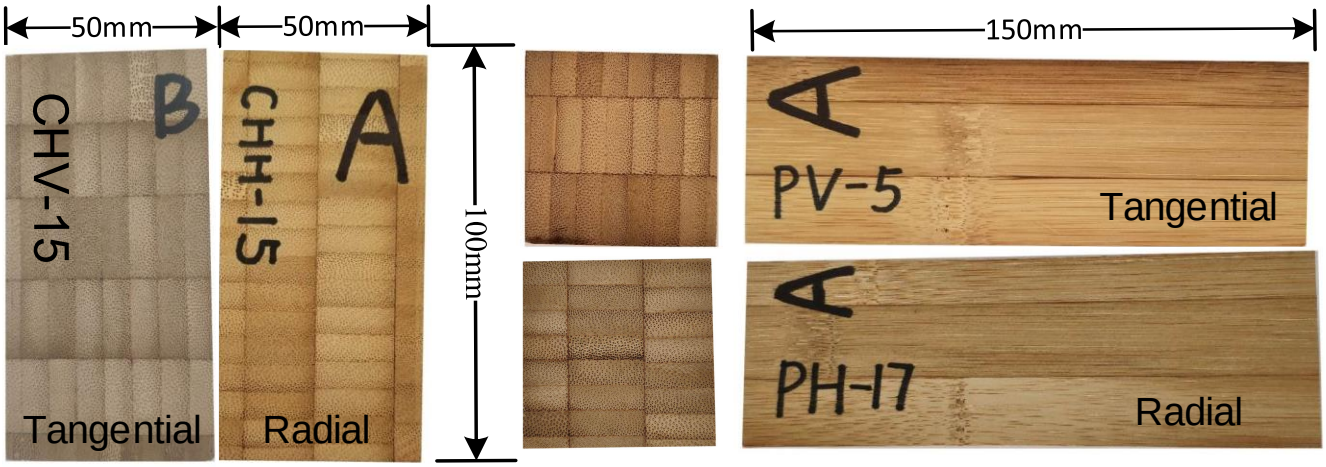

Figure 2 Transverse compression specimens

2.3 Testing procedures

Schematic diagrams for considered tests are shown in Figure 3. They were conducted using a 200-ton microcomputer controlled electro-hydraulic servo universal testing machine. Axial displacements were measured by displacement meters with data collection through TDS-530 data acquisition instrument. For specimens subjected to entire-surface compression, compressive strain values were captured by four pairs of strain gauges pasted on four side surfaces (8 strain gauges in total, as shown in Figure 3a). Partial compressive loading was applied using a steel block (50mm×75mm×25mm), and contact area between steel block and specimen was 50 mm×50 mm. Moisture content and density of tested LBL specimens were 7.0% and 736kg/m3, respectively.

Since there is lack of testing standard for engineered bamboo products, current loading systems were designed according to GBT50329-2012 for timbers. The displacement-controlled load at the speed of 2 mm/min was adopted. All tests were conducted in the structural laboratory of Nanjing Forestry University at ambient temperature of 24℃ and humidity of 60%.

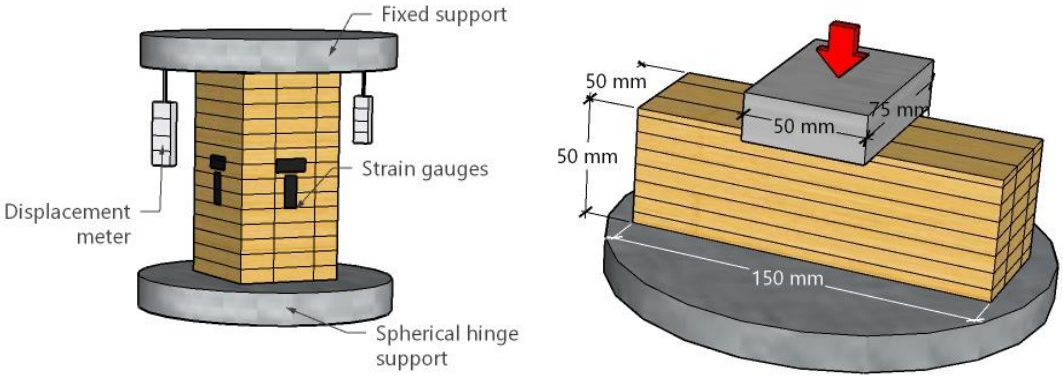

(a) Entire-surface compression (b) Local-surface compression

Figure 3 Test setup

2.4 Determination of proportional limit point

GBT 50329-2012 Chinese standard for test methods of timber structures specifies the method for determining proportional limit point for specimen under transverse compression: the tangent value of the angle between the tangent of the proportional limit point and the load axis shall be 1.5 times of the tangent value of the angle between the straight line and the load axis in the linear elastic stage, as shown in Figure 4.

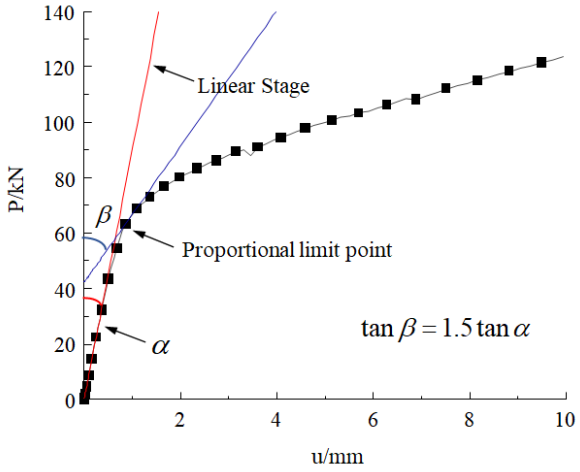

Figure 4 Schematic diagram of proportional limit point

The proportional limit strength can be calculated according to Equation (1):

$$f_e = \frac{F_e}{bl} \tag{1}$$

where f_e is the proportional limit strength, F_e is the proportional limit load, b is the width of specimen, l is the contact length.

2.5 Finite element method

2.5.1 Failure criterion and constitutive model

Although laminated bamboo lumber is a typical anisotropic bio-based material, it could be simplified as an orthotropic material to reduce the complexity in current study. Finite element analyses are conducted using ABAQUS/Standard following Hill failure criterion and ideal elastoplastic constitutive model, which have been successfully implemented in authors' previous work (Hong et al. 2021b; a) and proven to be valid for LBL. Equation (2) can be used to express Hill failure criterion.

$$F(\sigma_{ij}) = \sqrt{\begin{matrix} F\left(\sigma_{22}-\sigma_{33}\right)^2 + G\left(\sigma_{33}-\sigma_{11}\right)^2 + H\left(\sigma_{11}-\sigma_{22}\right)^2 \\ +2L\sigma_{23}^2 + 2M\sigma_{31}^2 + 2N\sigma_{12}^2 \end{matrix}} < \sigma^0 \tag{2}$$

where F, G, H, L, M, N are constants determined by the strength of material, which can be calculated by Equations (3)~(8):

$$F = \frac{\left(\sigma^0\right)^2}{2}\left(\frac{1}{\bar{\sigma}_{22}^2}+\frac{1}{\bar{\sigma}_{33}^2}-\frac{1}{\bar{\sigma}_{11}^2}\right) = \frac{1}{2}\left(\frac{1}{R_{22}^2}+\frac{1}{R_{33}^2}-\frac{1}{R_{11}^2}\right) \tag{3}$$

$$G = \frac{\left(\sigma^0\right)^2}{2}\left(\frac{1}{\bar{\sigma}_{33}^2}+\frac{1}{\bar{\sigma}_{11}^2}-\frac{1}{\bar{\sigma}_{22}^2}\right) = \frac{1}{2}\left(\frac{1}{R_{33}^2}+\frac{1}{R_{11}^2}-\frac{1}{R_{22}^2}\right) \tag{4}$$

$$H = \frac{\left(\sigma^0\right)^2}{2}\left(\frac{1}{\bar{\sigma}_{11}^2}+\frac{1}{\bar{\sigma}_{22}^2}-\frac{1}{\bar{\sigma}_{33}^2}\right) = \frac{1}{2}\left(\frac{1}{R_{11}^2}+\frac{1}{R_{22}^2}-\frac{1}{R_{33}^2}\right) \tag{5}$$

$$L = \frac{1}{2}\left(\frac{\tau^0}{\bar{\sigma}_{23}^2}\right)^2 = \frac{3}{2R_{23}^2} \tag{6}$$

$$M = \frac{1}{2}\left(\frac{\tau^0}{\bar{\sigma}_{13}^2}\right)^2 = \frac{3}{2R_{13}^2} \tag{7}$$

$$N = \frac{1}{2}\left(\frac{\tau^0}{\bar{\sigma}_{12}^2}\right)^2 = \frac{3}{2R_{12}^2} \tag{8}$$

where $\bar{\sigma}_{ii}$ are material strength in the three directions, $\bar{\sigma}_{ij}$ are shear strength, σ^0 is reference yielding stress, $\tau^0 = \sigma^0/\sqrt{3}$. R_{ij} can be calculated by Equations (9):

$$R_{11} = \frac{\bar{\sigma}_{11}}{\sigma^0}, R_{22} = \frac{\bar{\sigma}_{22}}{\sigma^0}, R_{33} = \frac{\bar{\sigma}_{33}}{\sigma^0}, R_{12} = \frac{\bar{\sigma}_{12}}{\tau^0}, R_{13} = \frac{\bar{\sigma}_{13}}{\tau^0}, R_{23} = \frac{\bar{\sigma}_{23}}{\tau^0} \tag{9}$$

Adopted ideal elastoplastic constitutive model is shown in Figure 5a, where X_t and X_c are the tensile

strength and compressive strength of LBL in grain direction (*L*); Y_t and Y_c are the tensile strength and compressive strength in radial direction (*R*); Z_t and Z_c are the tensile strength and compressive strength in tangential direction (*T*), respectively. The definition of directions L (1), T (2) and R (3) is shown in Fig. 5b. Table 2 summarizes all relevant constitutive model parameters from literature (Hong et al. 2021b; a; Tang et al. 2019; Wang et al. 2021b). It should be noted that the tensile properties are not used to calculate parameters in Hill failure criterion (Jasieńko et al. 2010), and the transverse mechanical properties are obtained from the current experimental works.

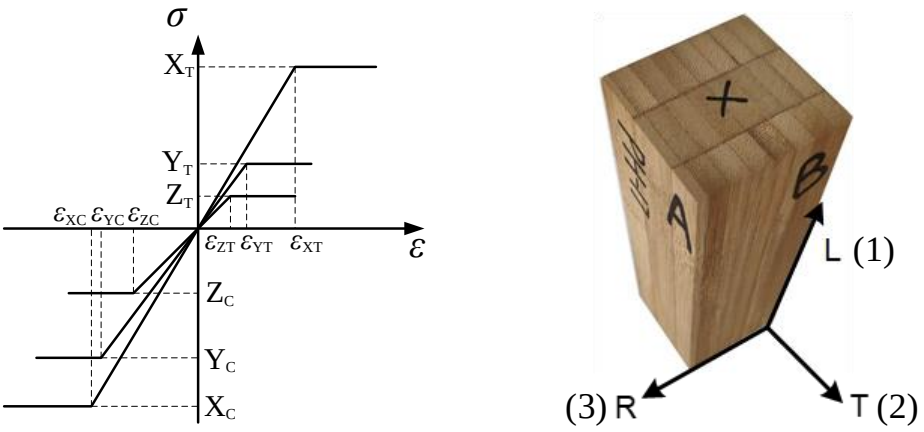

Figure 5 (a) Ideal elastoplastic constitutive model (b) L, T and R direction

Table 2 Constitutive model parameters

Elastic modulus（MPa）		Poisson's ratio		Strength（MPa）			
E_1	6323.7	μ_{12}	0.25	X_T	98	S_{XY}	18.13
E_2	1440	μ_{21}	0.053	Xc	59.63	S_{YZ}	22.59
E_3	1149	μ_{13}	0.2	Y_T	8.26	S_{ZX}	6.58
G_{12}	1365.08	μ_{31}	0.04	Y_C	21.63	σ^0	19.62 (for radial direction)
G_{23}	461.81	μ_{23}	0.42	Z_T	8.26	σ^0	21.63 (for tangential direction)
G_{13}	1260.09	μ_{32}	0.42	Z_C	19.62		

2.5.2 Modeling details

As shown in Fig. 6, the models of laminated bamboo specimens, steel block and bottom plate are created.

The surface-to-surface contact is used to simulate the interface between specimen, steel block and bottom plate. The normal direction of the interface is defined as hard contact, which allows the interface to separate during stretching and not penetrate during compression. The tangential behavior of the interface along the normal direction is simulated by the coulomb friction model. After conducting tests of friction coefficient influence on simulation results (0.1, 0.3 and 0.5), it is found that friction coefficient of 0.3 matches the experimental results best. Therefore, the friction coefficient is set as 0.3.

Reference points (RP) are created for the model to apply load and constrains. For entire-surface compression specimens, the coupled constrains are set to apply the displacement-controlled loads. U1, U2, and U3 are restrained on the bottom ends, while the top end is fixed. For local-surface compression specimens, it should be noted that since the load-displacement curves were obtained using machine data directly, the initial stiffness is lower than the real condition because of additional displacement from gaps in machine. Thus, the elastic boundary conditions are applied to the finite element model to make the simulated stiffness consistent with the test stiffness. According to the debugging results, the elastic modulus and Poisson's ratio of the steel block are set as 666 MPa and 0.3, respectively. The coupled constrains are set on the steel block to apply the displacement-controlled loads, while the rigid constrains are set to bottom steel plate and ignore its influence. Both ends are fixed according to the condition of experiment. The type of solid elements is Standard/C3D8. The meshing density for specimens and steel members is 2 mm. The calculation step is set to 1s, and the displacement-controlled loads of 20 mm are loaded through the smooth analysis step.

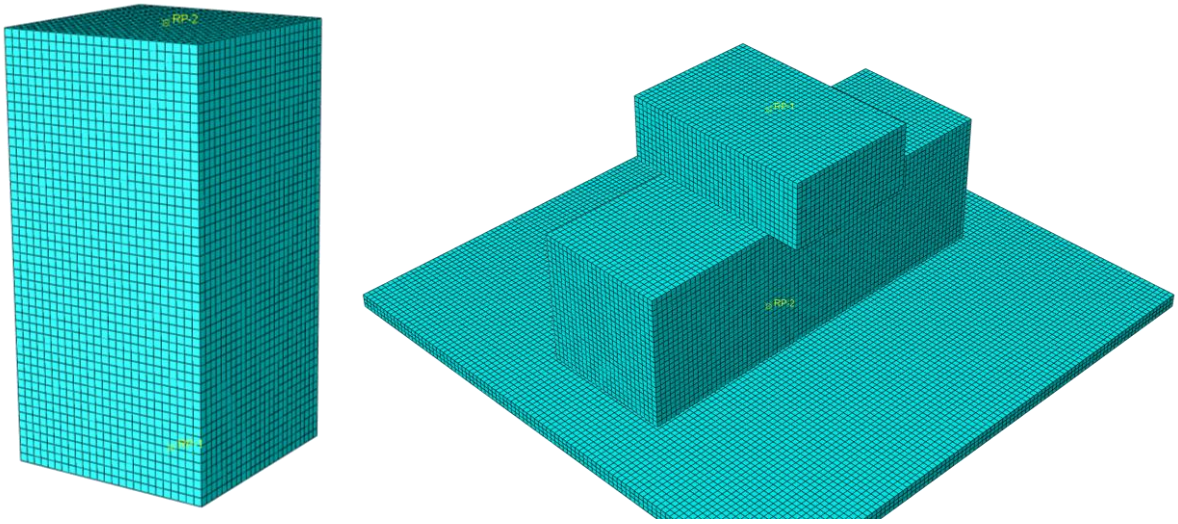

(a) Entire-surface compression specimen (b) Local-surface compression specimen

Figure 6 Meshing of model

In the following section, the failure phenomena of the specimens under entire-surface compression and local-surface compression are described and analyzed firstly. Meanwhile, results obtained from finite element method are presented along with test results to validate the FEA model. The data obtained from the tests are analyzed and discussed. Then, the vertical stress (stress throughout thickness) caused by local compression is calculated and compared with FEA results to explain the mechanism of enhancement in proportional limit strength. Next, the correlation between the bearing capacity and the displacement of the specimens under local compression in the elastic deformation stage is derived. At last, parameter studies are carried out using finite element method.

3. Experimental and finite element analysis

3.1 Load-displacement curves and failure patterns

3.1.1 Entire-surface compression specimens

Load-displacement curves and typical failure patterns for entire-surface compression specimens are shown in Figure 7 and 8, respectively. Obtained curves can be divided into three segments i.e., bi-linear stages and descending stage.

At the beginning of loading, the specimen is in the initial elastic stage with limited deformation; no

obvious phenomenon can be observed on the surface. As the load continues increasing, the specimen enters the second linear stage and begins to yield. Several micro cracks initially appear at the splice interfaces and the horizontal splice lines are no longer straight. Obvious deformation can be observed at this phase. These cracks then extend from the central part of the specimen to the side surfaces along inclined 40-70 degrees direction (Figure 8a~d) before reaching the corner of the specimen which results in the final failure. Similar observation was also reported by Tinkler-Davies et al. (Tinkler-Davies and Shah 2021) i.e. a 40-60 degrees shear face was occurred from the upper-right corner leading towards to the bottom left during loading (Figure 8e, Strain of 10% from DIC).

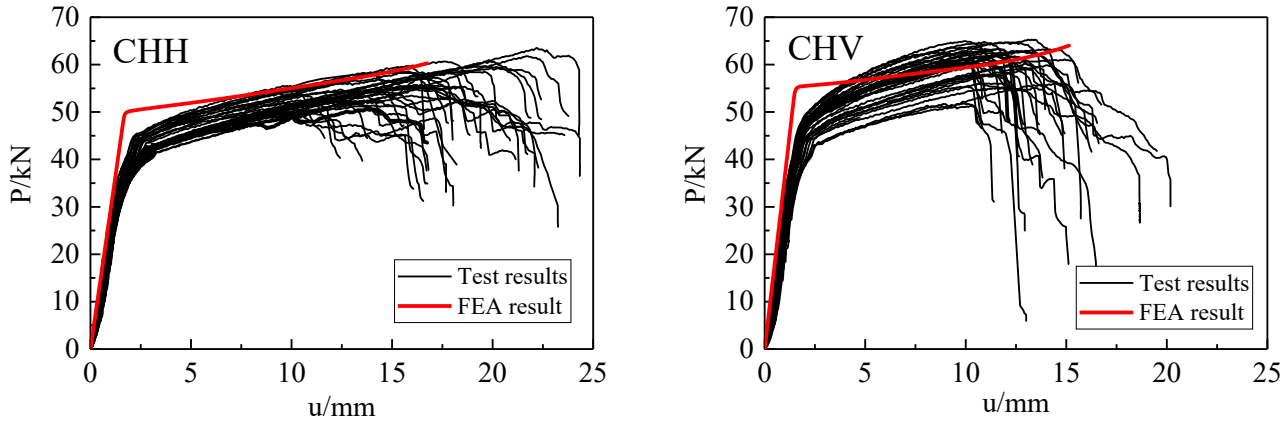

(a) CHH (b) CHV

Figure 7 Load-displacement curves

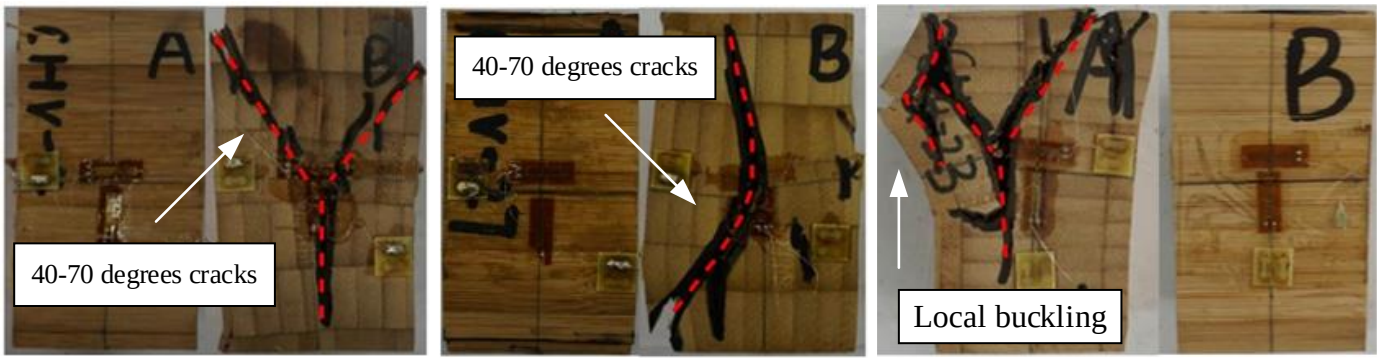

(a) CHV-4 (b) CHV-27 (c) CHH-23

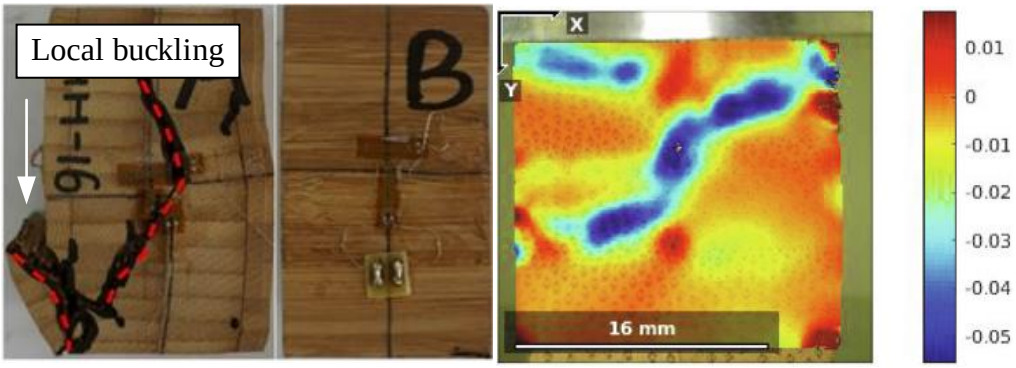

(d) CHH-16 (e) Compressive strain of 10% from DIC

Figure 8 Observed failure modes for CHV and CHH groups

The propagation of cracks along the inclined 40-70 degrees could be explained by Poisson's ratio in Plane TR (23) and RT (32). u_{23} and u_{23} are 0.42. Therefore, the tangential value of the angle between the sum of lateral and vertical strain vectors and the horizontal line is tan (1/0.42), which corresponds to approximate 67.22°. During the failure process, it is found that the cracks always occurred firstly in Plane TR and RT. This phenomenon could also be attributed to Poisson's ratio. It is shown in Table 2 that u_{23} and u_{23} is much higher than u_{21} and u_{31}, which means lateral deformation of specimens parallel to axis 2 and 3 is much larger (about 10 times) than that parallel to axis 1, so the cracks always occurred firstly in Plane TR and RT.

Obvious local buckling occurred along the glue lines in almost every specimen in CHH group, but rarely occurred in specimens within CHV group. The arrangement of bamboo laminates could be closely related to this phenomenon, as can be seen in Figure 9; the thickness of bamboo strips at the edge layer of CHV is close to that at the middle layer, whereas at the edge layer of CHH, the thickness of bamboo laminates is far from that at the middle layer. The edge layer of CHH specimen is relatively weak, compared with CHV specimen, the load cannot be distributed uniformly so the specimen is easy to crack during load transmission and has a high probability to occur local buckling. However, Figure 6 shows that obviously higher ductility is observed for CHH when compared with CHV, which could also be attributed to the arrangement of bamboo laminates.

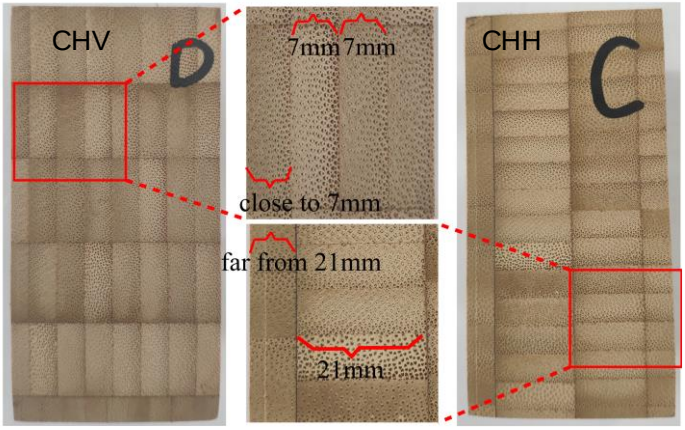

Figure 9 Different arrangement of bamboo laminates between CHV and CHH

3.1.2 Local-surface compression specimens

Load-displacement curves and typical failure modes for local compression specimens are shown in Figure 10 and 11, respectively. Curves show a bi-linear characteristic. Exposed to local compression perpendicular to the grain, laminated bamboo lumber behaves high ductility and extensive deformation capability.

In the initial stage, no significant change could be found on the surface with increasing in load. However, when PV specimen enters the second linear stage, several horizontal cracks near the splice lines appear firstly, with the two ends of the specimen tilte upward. Meanwhile, plastic deformations could be observed on the specimen near the sharp edge of steel block. As the axial displacement increases, the loading area under the steel block is gradually compacted following by considerable vertical cracks on the two end surfaces. Finally, the test is stopped manually, as the load can continue to grow without limit. It can be found that the side surfaces (A, C) nearly fall off from the main body, which is also clearly showed in the FEA results.

The test phenomenon of PH specimen is similar to that of PV. After the plastic deformation occurs at the contact edge between the steel block and the specimen, horizontal cracks firstly appear at both ends. With the increase of load, the cracks gradually develop to the inside, and the width of cracks also become larger. Compared with PV specimen, most of PH specimens maintain a better integrity, and there is no obvious falling off trend of side surfaces. As illustrated in Figure 10, the linear stage's range is just approximately 1 mm,

which is negligible in the real item. Therefore, the deformation or stiffness of LBL components should be carefully regulated throughout design.

Curves from developed FE technique for PH and PV specimens are shown in Figure 10 as well. This model provides a reasonable prediction, especially for PH group. However, FEA results overestimates test results for PV group. The discrepancy may be explained by the reason that smaller effective bearing area in PV group due to the side surfaces separation of the specimen during loading. These changes in invalid parts are not considered in finite element model.

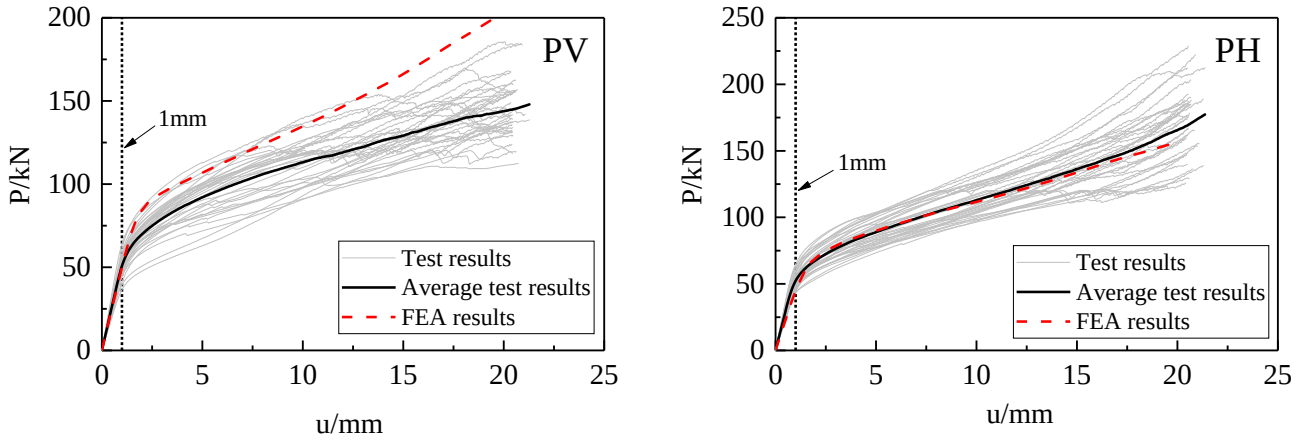

(a) PV (b) PH

Figure 10 Load-displacement curves

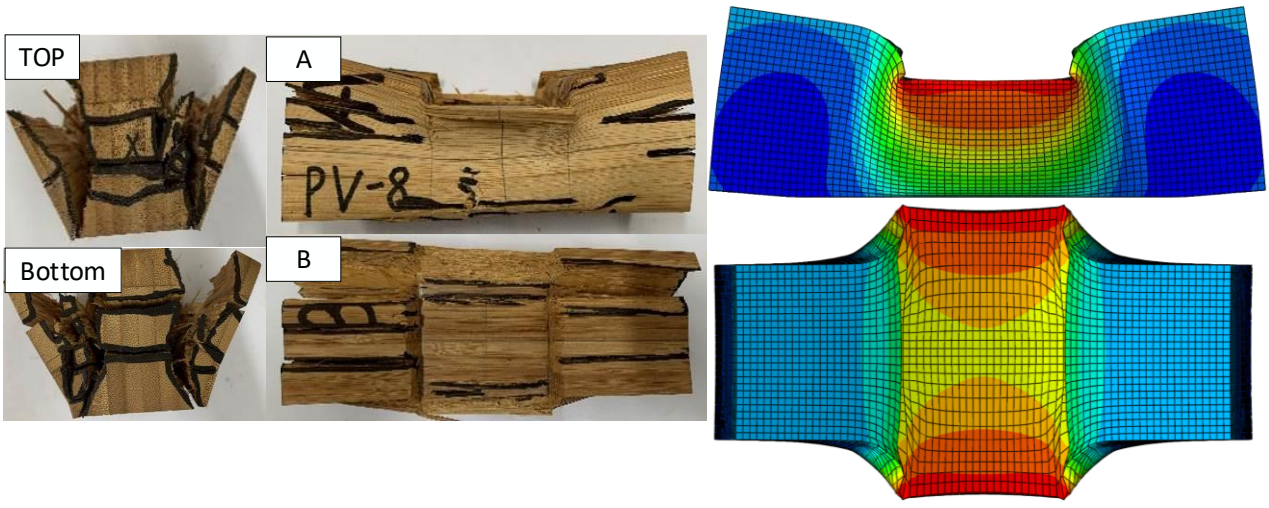

(a) PV-8

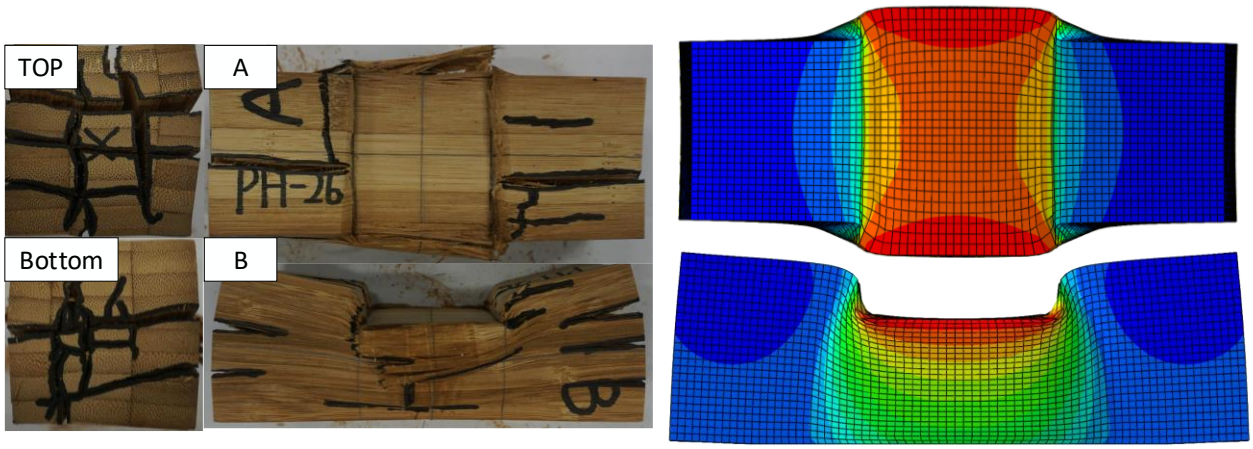

(b) PH-12

Figure 11 Observed failure modes for PV and PH groups

3.2 Analysis of test results

3.2.1 Basic mechanical properties

A summary of main test results is presented in Table 3. P_{max} is the ultimate bearing capacity of specimen recorded by the data acquisition. f_c is the compressive strength calculated by P_{max}/A, where A is the cross-sectional area. E_c is the elastic modulus and μ_c is the Poison's ratio, and they were calculated in the linear elastic region.

Test data in Table 3 show relevant coefficient of variation (COV) is basically less than 20% confirming reliable results obtained from current setup. Different Poison's ratios in different plane are observed confirming laminated bamboo lumber as an anisotropy material, however, these properties are basically same between two transverse directions. In terms of compressive strength and elastic modulus, tangential direction shows slightly higher values than radial direction. Their relation can be roughly considered as:

$$E_T = 1.1E_R \tag{10}$$

$$f_T = 1.1f_R \tag{11}$$

where T and R means tangential direction and radial direction, respectively.

Dixon (2017) studied the effect of density on the compressive strength of moso bamboo in tangential and radial direction. It is found that the compressive strength in the tangential direction is similar to that in the

radial direction, which is roughly constant at about 20 MPa and independent of density. The strength value is consistent with results in current study. However, in our study, average value and characteristic value both show that the strength and elastic modulus are higher in tangential direction. This may attribute to the densification (hot/cold pressing) in the process of laminated bamboo lumber. As illustrated in Section 2.1, the hot pressure technique implemented the pressure of 9 MPa for upper and lower surfaces and 6.5 MPa for left and right surfaces, which indicates that the structure of bamboo may be denser in the tangential direction. These speculations need further confirmation in the future. Nevertheless, due to the fact that densification is an important phenomenon in the processing of some structural bamboo products, determining optimal densification methods and levels would be beneficial (Dixon 2017).

In practical application, the transverse direction setup should be used with caution. As already discussed, failure phenomena are different between specimen groups although their mechanical behavior seems to be similar. Considering the better ductility and sample integrity during failure process, the author recommends to choose radial direction for local compression in the construction.

Table 3 Main test results

	Group	P_{max} /kN	f_c /MPa	E_c /MPa	μ_c (A/C)	μ_c (B/D)
CHH	Mean value	55.68	21.74	1550	0.529	0.06
	Coefficient of variation	6%	5%	14%	10.9%	21%
	Standard deviation	3.60	1.15	217	0.058	0.01
	Characteristic value	49.03	19.62	1149	0.42	0.04
CHV	Mean value	60.65	24.09	1700	0.073	0.53
	Coefficient of variation	6%	6%	8%	15.5%	11%
	Standard deviation	3.43	1.33	141	0.011	0.06
	Characteristic value	54.32	21.63	1440	0.053	0.42

Note: The characteristic values are calculated as the 5-percentile value under 75% confidence level, referring to ASTM D2915_17. Characteristic value = Mean value − 1.846 ∗ Standard deviation.

3.2.1 Stress-strain behavior

Figure 12 shows the stress-strain behavior of CHH and CHV specimens. There is no descending stage since the strain gauges were broken due to the damage or deformation of specimens. It can be seen that the curves can be divided into two segments, which are elastic stage and plastic stage. The Ramberg-Osgood relation is commonly used to describe the stress-strain behavior without distinct yield point. Its expression is:

$$\frac{\varepsilon}{\varepsilon_0}=\frac{\sigma}{\sigma_0}+\alpha\left(\frac{\sigma}{\sigma_0}\right)^n \tag{12}$$

where ε is strain; σ is stress; α and n are fitted parameters; ε_0 and σ_0 are test data at any point in the elastic region. Thus, the stress-strain behavior of CHH and CHV can be obtained:

$$\frac{\varepsilon}{0.003}=\frac{\sigma}{5.33}+0.018\left(\frac{\sigma}{5.33}\right)^{4.46},\ \text{for CHH} \tag{13}$$

$$\frac{\varepsilon}{0.003}=\frac{\sigma}{5.88}+0.012\left(\frac{\sigma}{5.88}\right)^{4.34},\ \text{for CHV} \tag{14}$$

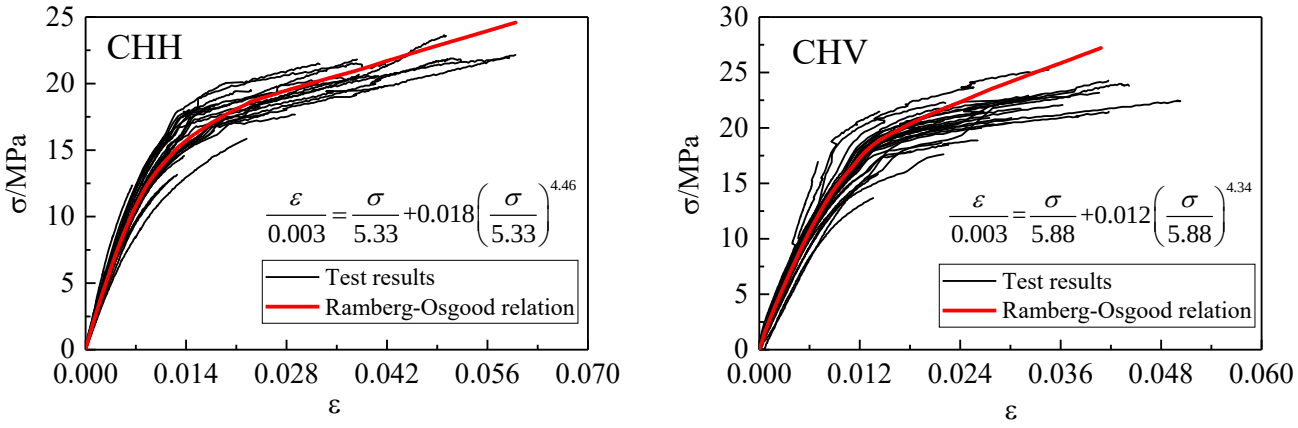

(a) CHH (b) CHV

Figure 12 Stress-strain curves

3.2.2 Proportional limit point

Results obtained from average curves are showed in Figure 13 and Table 4. It is found that the

proportional limit strength of PH and PV are 1.63 times and 1.67 times higher than that of CHH and CHV, respectively. Also, the strength in the tangential direction is higher than that in the radial direction, which is consistent with the findings in basic mechanical properties.

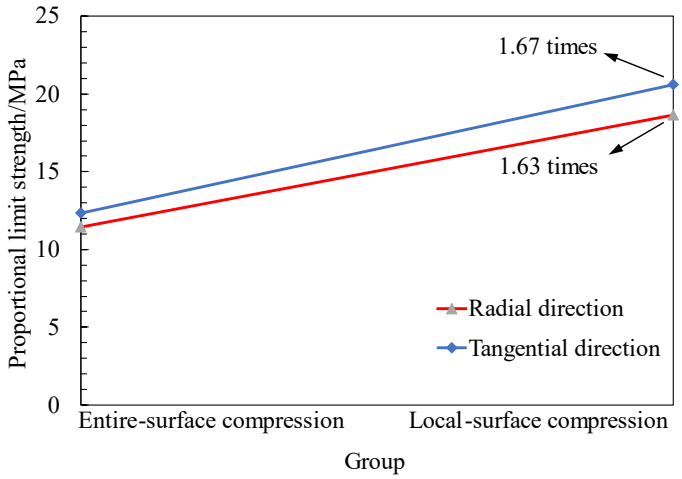

Figure 13 Proportional limit strength

Table 4 Parameters for proportional limit point

Group	$\tan(90-\alpha)$	$\tan\alpha$	$\tan(90-\beta)$	$\tan\beta$	Proportional limit point (u, P)	f_e/MPa	SI
CHH	30.4387	0.0329	20.2429	0.0494	(1.20, 28.54)	11.42	-
CHV	34.3279	0.0291	22.8833	0.0437	(1.11, 30.84)	12.34	-
PH	59.3035	0.0169	39.3700	0.0254	(0.83, 46.68)	18.67	1.63
PV	52.5170	0.0190	35.0877	0.0285	(1.02, 51.48)	20.59	1.67

Note: SI is strength index, which means the promotion ratio of proportional limit strength. It is calculated by dividing the proportional limit strength of local-surface compression specimen by that of entire-surface compression specimen.

3.3 Calculation of vertical stress under local compression

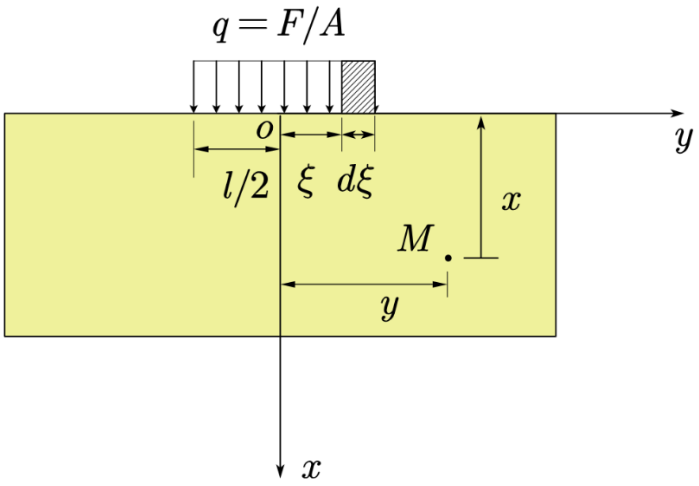

Figure 14 Calculation diagram

Uneven vertical stress (stress throughout thickness) caused by local compression on the specimen is necessary to study. Referring to Elasticity (Barber 2002), when a half-plane body is subjected to a normal concentrated force on the boundary, the vertical stress in the rectangular coordinate are:

$$\sigma_x = -\frac{2F}{\pi}\frac{x^3}{\left(x^2+y^2\right)^2} \tag{15}$$

In these tests, the specimens were subjected to distributed force. The vertical stress can then be obtained by superposition. As shown in Figure 14, to obtain the stress values at point M (x, y), we can take the length $\mathrm{d}\xi$ and consider the force $\mathrm{d}F = q\mathrm{d}\xi$ applied to it as a small concentrated force. The vertical and horizontal distances of M from the concentrated force $\mathrm{d}F$ are x and $y-\xi$, respectively. Therefore, the stress components induced by $\mathrm{d}F$ at point M are:

$$\mathrm{d}\sigma_x = -\frac{2q\mathrm{d}\xi}{\pi}\frac{x^3}{\left[x^2+(y-\xi)^2\right]^2} \tag{16}$$

To obtain the stress components caused by all distributed forces, it is necessary to superimpose the stress caused by all small concentrated forces. We can get:

$$\sigma_x = -\frac{2F}{\pi A}\int_{-l/2}^{l/2}\frac{x^3\mathrm{d}\xi}{\left[x^2+(y-\xi)^2\right]^2} \tag{17}$$

Figure 15 and 16 illustrate the comparison of FEA findings (PH group) with computed results. The stress distribution along the height direction is depicted in Figure 15. At 47.26 kN, the results are extracted and computed. As can be observed, the farther the specimen is from the location where the load is applied, the less

stress is applied to the specimen. However, when the position is close to the steel block and bottom plate, the FEA stress values are increased, owing to the friction effect between the specimen and the steel parts. This effect is reduced when the position is removed from the steel block (Figure 15b), at which point the estimated values correspond well with the FEA results. At the position of the center nodes, the computed compressive stress values are greater than the FEA values, indicating that the load is scattered outside in the vertical direction, thus reducing the stress.

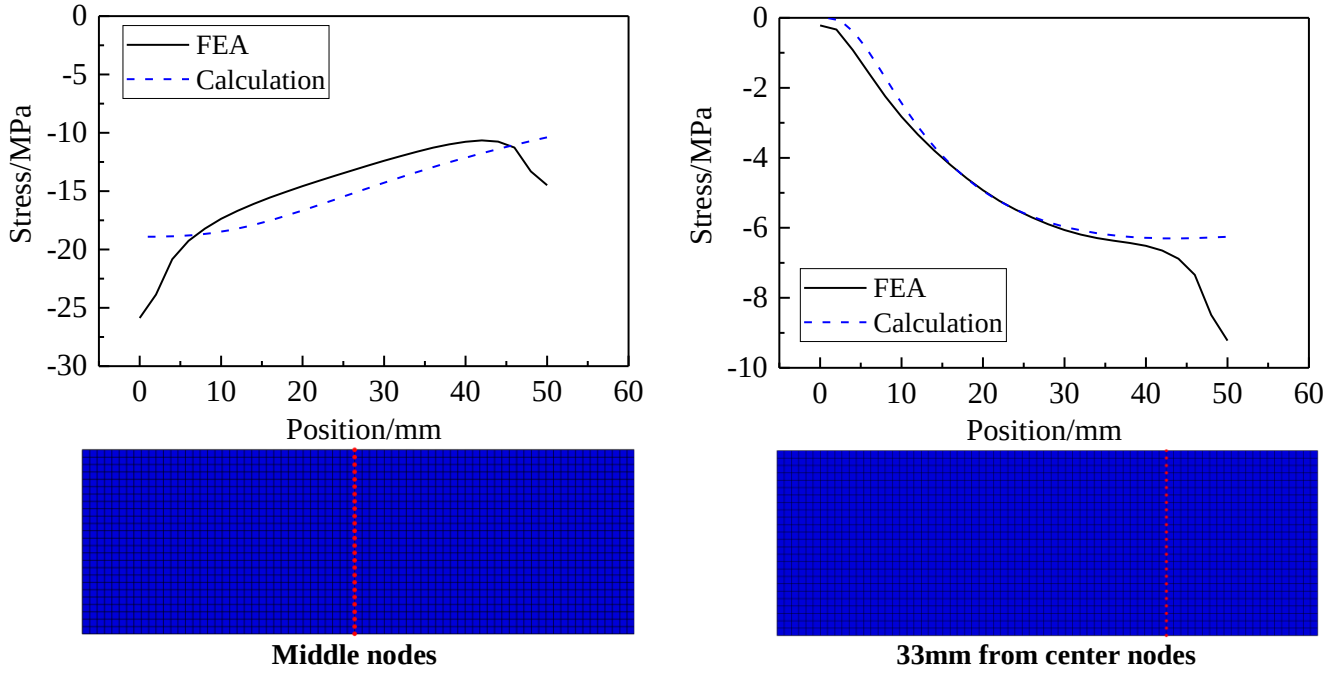

(a) Middle position (b) 33mm from center nodes

Figure 15 Results along the height direction at 47.26 kN

The stress distribution along the length direction is depicted in Figure 16. At 11.39 kN, the results are extracted and computed. As illustrated in Figure 16a, the sharp edges of the steel block at -25 mm and 25 mm create stress concentrations, commensurate with the reported failure pattern. Both the FEA and computed results reveal that the locally applied load has an effect greater than 50 mm. The FEA results are greater than the calculated values, indicating that Equation 16 is unsuitable for use near the edge. However, it may provide a useful general change pattern that aids in understanding the stress distribution. At a distance of 25 mm from the uppermost surface nodes, the stress concentration effect of the steel block's sharp edge and the friction effect dissipate. Calculated and FEA stress values become much more consistent. However, the computed values are still greater than the FEA results within the range of -25 mm to 0 mm, demonstrating once again that the load is scattered outside in the vertical direction.

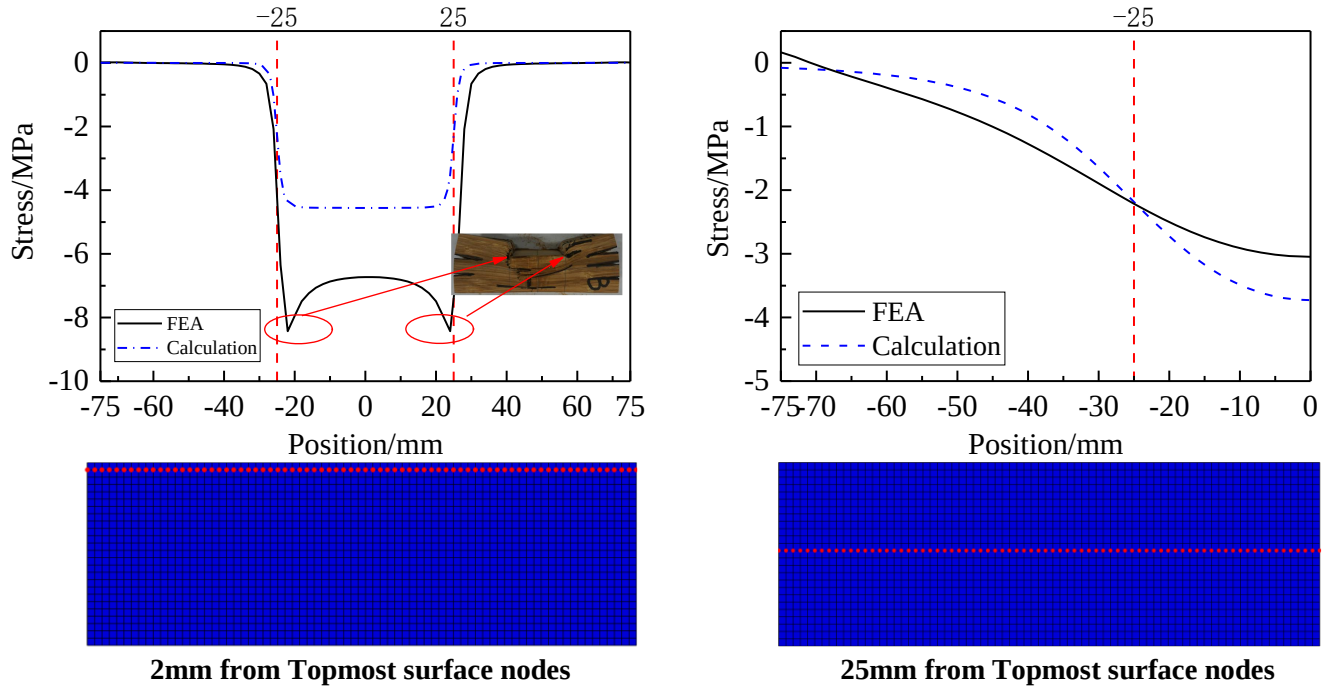

(a) 2mm from topmost surface (b) 25mm from topmost surface

Figure 16 Results along the length direction at 11.39 kN

The reason for proportional limit increased of local surface compression specimen could be drawn. In the vertical direction (within the range of -25 mm to 25 mm), the external load is dispersed significantly thus effectively reduce the vertical stress, as shown in Figure 15b and Figure 16b. Therefore, under the same load level, the deformation of local compression specimen is smaller than that of entire compression specimen, which means the yield stress of LBL can only be achieved under greater external load. As a result, the proportional limit point derived from load-displacement curves of local-surface compression specimens is enhanced.

3.4 Prediction of bearing capacity in elastic stage

It is foreseeable that once the dimension of steel block or specimen changes, the relationship between bearing capacity and vertical displacement will change significantly. Therefore, it is inappropriate to directly fit the relationship based on test data (Zhou et al. 2021), as the results can only be applied for the same dimension. To obtain a more reasonable calculation formula, the relationship between displacement and load is derived, taking into account the contact length l between steel block and specimen, as well as the height H, the length L and width b of specimen (Figure 17a).

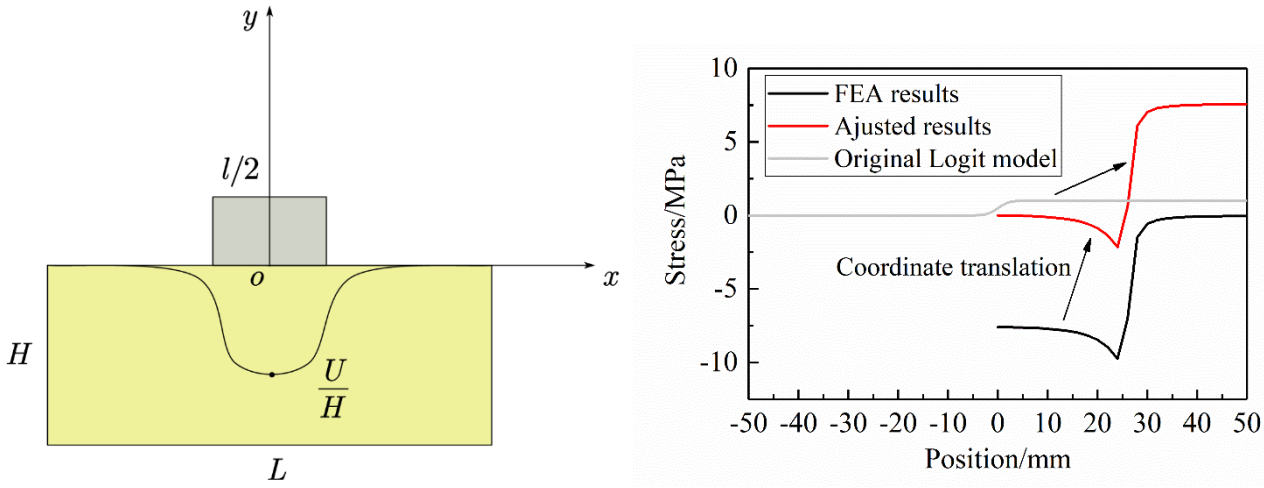

Figure 17 (a) Calculation diagram (b) Coordinate translation

In the linear elastic stage, the strain at the center of the specimen under the steel block is:

$$\varepsilon_{\max} = \frac{\sigma_{\max}}{E} = -\frac{u}{H} \tag{18}$$

where， $\varepsilon_{\max}$ is the maximum vertical strain， $\sigma_{\max}$ is the corresponding maximum vertical stress, u is the vertical displacement， H is the height of the specimen, E is the transverse elastic modulus.

According to the FEA results, it is clear that the shape of vertical stress distribution basically follows Logit model (Cramer 2003), which is a discrete choice model popular in statistics area. Its functional model is:

$$y = \frac{e^x}{1+e^x} \tag{19}$$

Through coordinate translation (Figure 17b), we can express the stress distribution under local compression by Logit model:

$$\varepsilon + \frac{u}{H} = \frac{u}{H}\frac{e^{x-l/2}}{1+e^{x-l/2}} \tag{20}$$

where ε is the vertical strain of specimen topmost surface， l is the length of steel block (i.e. the contact length)， x is the position of point between 0 and $l/2$. Therefore, the vertical strain is:

$$\varepsilon = -\frac{u}{H(1+e^{x-l/2})} \tag{21}$$

Then, the compressive force N exerted by steel block on the specimen is:

$$N = 2\int_0^{\frac{L}{2}} E\varepsilon b \mathrm{d}x \tag{22}$$

where E is the elastic modulus in the transverse direction, b is the width of specimen.

Substituting Equation (21) into Equation (22), and according to the principle of force balance, we can get:

$$P + 2Eb\int_0^{\frac{L}{2}}\left[-\frac{u}{H(1+e^{x-l/2})}\right]\mathrm{d}x = 0 \tag{23}$$

Finally, the relationship between the external load P and the vertical displacement u in the linear elastic stage is:

$$P = 2Eb\int_0^{\frac{L}{2}}\left[\frac{u}{H(1+e^{x-l/2})}\right]\mathrm{d}x \tag{24}$$

The analytical solution of Equation (24) cannot be obtained. According to Section 3.3, the stress out of range of contact length could be neglected. Therefore, Equation (24) could be simplified as:

$$P = 2Eb\int_0^{\frac{l}{2}}\left[\frac{u}{H(1+e^{x-l/2})}\right]\mathrm{d}x = \frac{2Eub}{H}\left[\frac{l}{2}+\ln(\frac{1+e^{-l/2}}{2})\right] = \frac{EA}{H}u + \frac{2Eub}{H}\ln(\frac{1+e^{-l/2}}{2}) \tag{25}$$

Where A is the bearing area.

Calculated results, test results, FEA results are shown in Figure 18. The elastic modulus used for PH and PV group are 1192 MPa and 1468 MPa, respectively. In FEA-2, the displacement results are obtained from topmost surface of specimens under the steel block, because the displacement from steel block cannot reflect the real situation when elastic boundary conditions are applied. As can be seen in Figure 18, the calculated results are slightly smaller than simulated results, which could be attributed to ignoring stress concentration. Although the proposed equations are applicable to some extent, they have some limitations. If the sample is slightly bigger than the bearing area, it may behave like an entire-surface compression specimen. Besides, if the bearing shape is circular, the stress distribution must be totally different. In the next section, some preliminary parameter studies are conducted to discuss these issues.

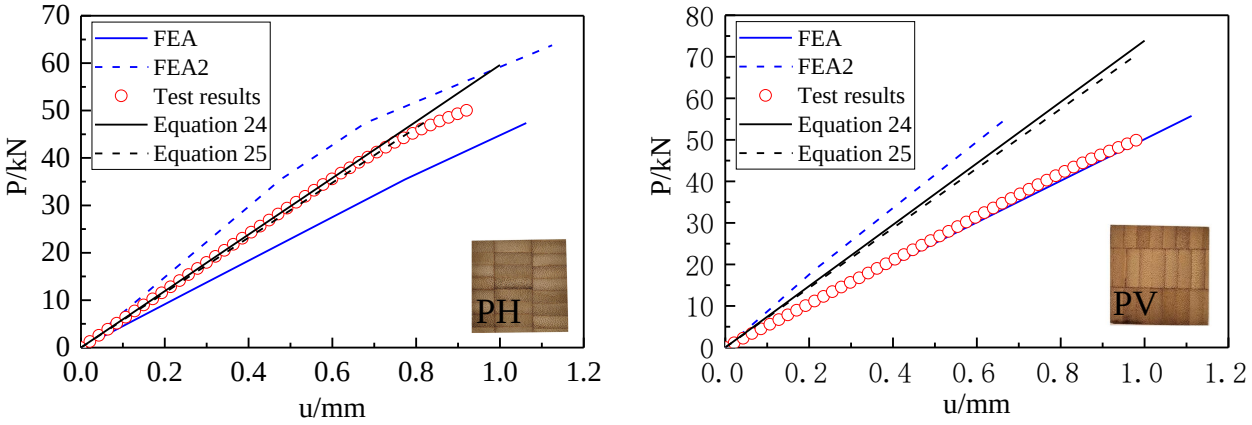

(a) PH (b) PV

Figure 18 Compared results

3.5 Parameter studies

To furtherly study the mechanical behavior of laminated bamboo lumber under different working conditions, the effects of bearing area, bearing shape and loading mode are discussed using finite element analysis method. The simulation works are conducted in the radial direction of LBL, because the FEA results of PH group are more consistent with test results. The boundary conditions are same as PH group. The calculation step is set to 1s, and the displacement-controlled loads of 3 mm are loaded through the smooth analysis step.

3.5.1 Effect of bearing shape on stress distribution

In practical engineering application, circular and rectangular shapes are widely used. Therefore, a circular steel block with dimension of Ø50 mm is set. The thickness of steel block is 25 mm. The load-displacement curve and vertical stress distribution curves are shown in Figure 19. The vertical stress distribution at the position of 0 mm, 12 mm and 25 mm are extracted. Similar to rectangular bearing shape, there are stress concentrations at the edge of steel block, and then the stress distribution becomes uniform. The significant difference is that the stress distribution along the width direction is various, so Equation (25) is not applicable in this case. At the position of 0 mm, there is only a narrow area that could bearing capacity.

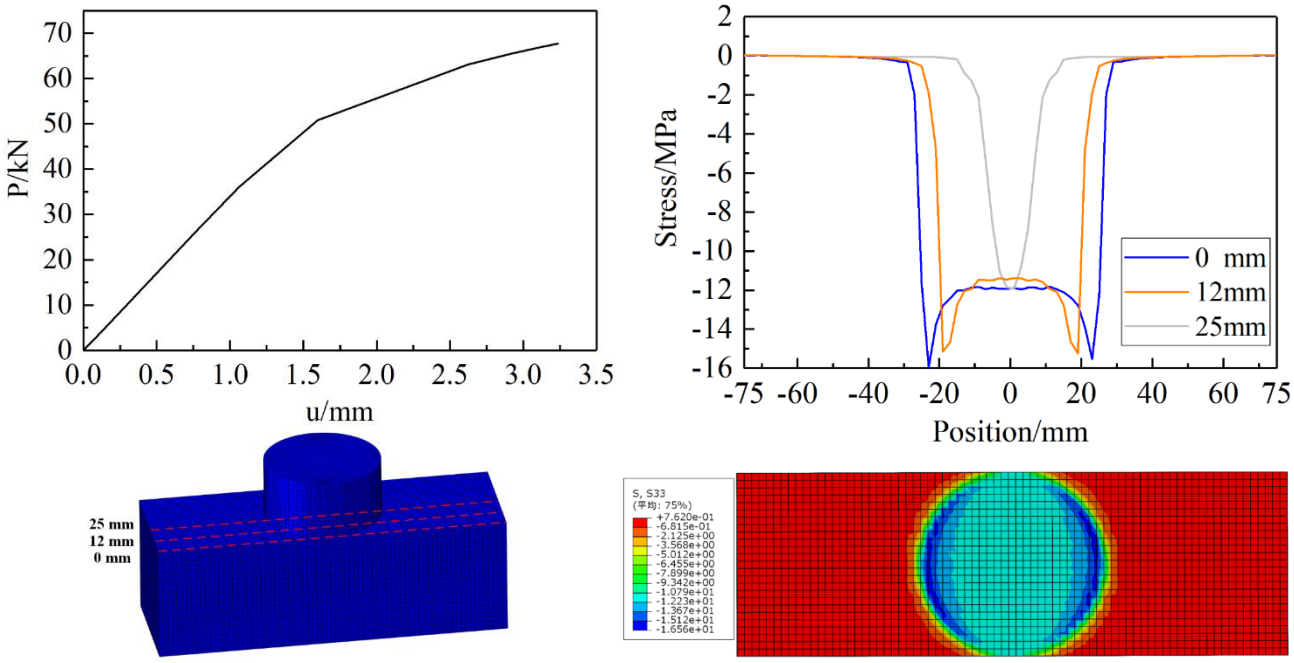

(a) Load-displacement curve (b) Vertical stress distribution

Figure 19 Results at 26.44 kN

The compressive force N exerted by circular steel block on the specimen should be:

$$N = 2\int_0^{\frac{l}{2}}\int_{-\frac{b}{2}}^{\frac{b}{2}} E\varepsilon \mathrm{d}x\mathrm{d}z \tag{26}$$

The change of contact length along the width direction l is:

$$l = 2\sqrt{r^2 - z^2} \tag{27}$$

Therefore, the compressive force exerted by circular steel block could be written as:

$$N = 2\int_0^{\sqrt{r^2-z^2}}\int_{-\frac{b}{2}}^{\frac{b}{2}} E\varepsilon \mathrm{d}x\mathrm{d}z \tag{28}$$

According to the principle of force balance, we can get:

$$P = -2\int_0^{\sqrt{r^2-z^2}}\int_{-\frac{b}{2}}^{\frac{b}{2}} E\varepsilon \mathrm{d}x\mathrm{d}z = \frac{2Eu}{H}\int_{-\frac{b}{2}}^{\frac{b}{2}}\left[\ln\left(\frac{1+e^{-\sqrt{r^2-z^2}}}{2}\right)+\sqrt{r^2-z^2}\right]\mathrm{d}z \tag{29}$$

The comparison of calculated results and FEA results is shown in Figure 20. Thus, if there is a known function which could describe the profile of the steel block, the load-displacement curve could be derived.

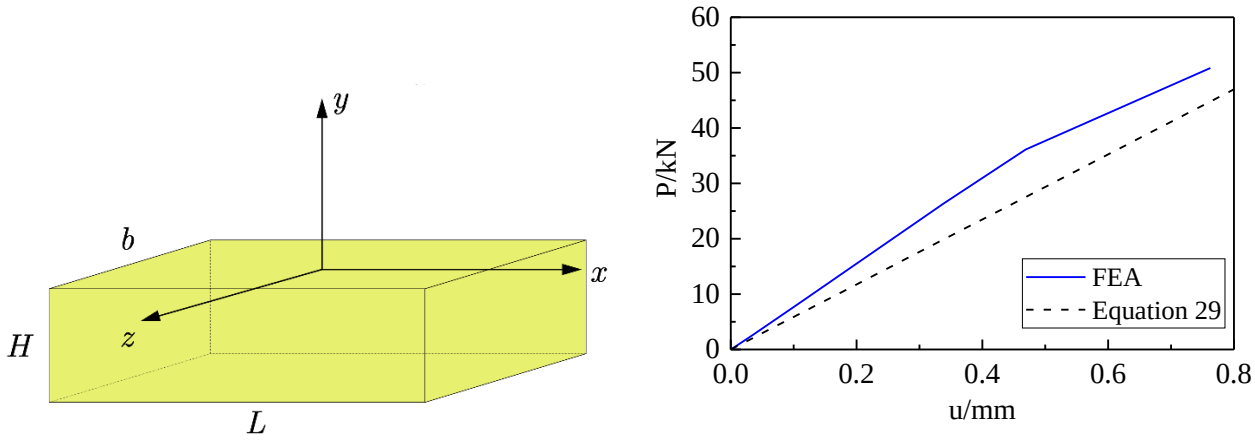

Figure 20 (a) Calculation diagram (b) Load-displacement curve

3.5.2 Effect of bearing area on bearing capacity

According to Equation (25), the bearing capacity will change approximately linearly with the change in bearing area. However, Equation (25) is derived under the condition of steel block could totally cover the specimen. If the specimen is slightly bigger than the bearing area, it may behave like an entire-surface compression specimen. To study this problem, the steel block is set as 48mm×48mm×25mm. Besides, a specimen with dimension of 48mm×48mm×50mm is created and compressed under the steel block with dimension of 80mm×80mm×25mm, as shown in Figure 21.

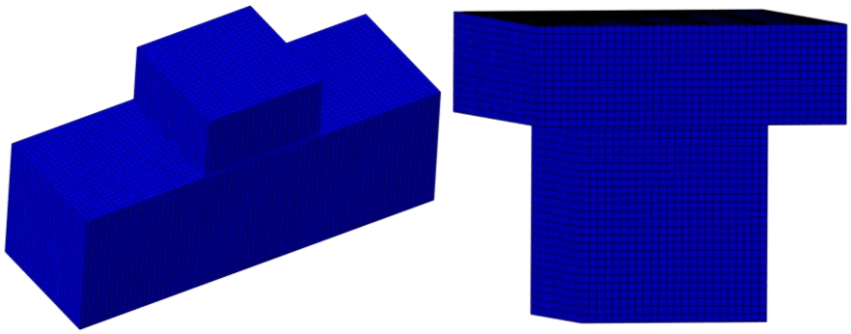

(a) Local compression (b) Entire compression

Figure 21 Finite element model

The load-displacement results and vertical stress distribution along the height direction are shown in Figure 22. It can be seen in Figure 22a that the load-displacement curves of two group are very consistent in the initial stage, which proves that specimen will behave like entire-surface compression specimen if the specimen is slightly higher than the bearing area. Besides, the friction effect between specimen and steel

members is largely diminished. However, the specimen under local compression still has higher bearing capacity due to the load dispersed mechanism. The stress distributions are extracted at the displacement of 0.77 mm. As can be seen in Figure 22b, the stress of local compression specimen gradually decreases, while that of entire compression specimen keeps unchanged except the part near the loading end. Therefore, even though their mechanical behaviors are similar, the specimen under local compression can still bear larger load.

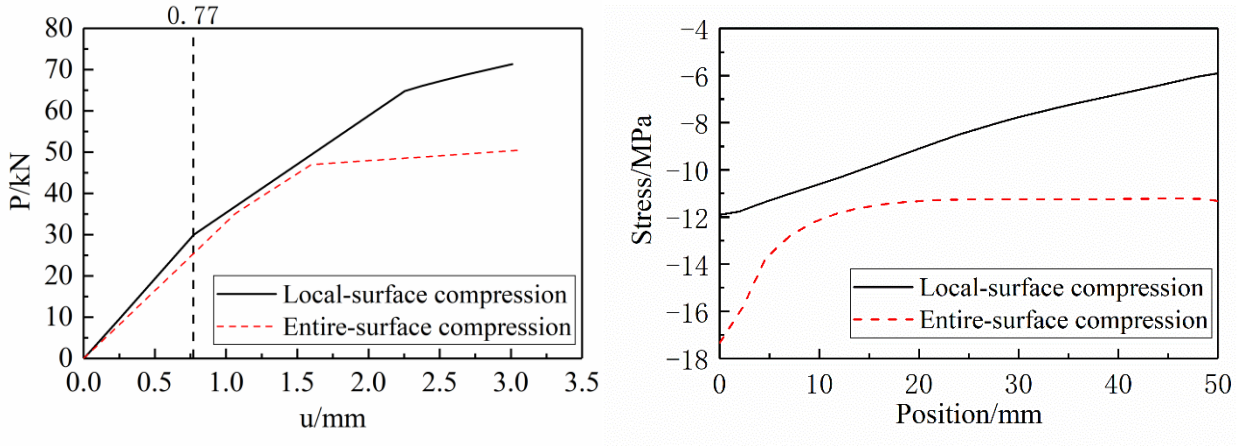

(a) Load-displacement curves (b) Load at displacement of 0.77 mm

Figure 22 Effect of bearing area on bearing capacity

3.5.3 Effect of loading mode on bearing capacity

Transverse compression of structural components can be divided into three types according to their loading mode (see Fig. 23), namely entire-surface compression, intermediate-surface local compression and end-surface local compression. In this section, effect of loading mode on bearing capacity was studied and the stress distribution under the steel block was compared. L (150 mm) and l (50 mm) are the length of specimen and steel block, respectively.

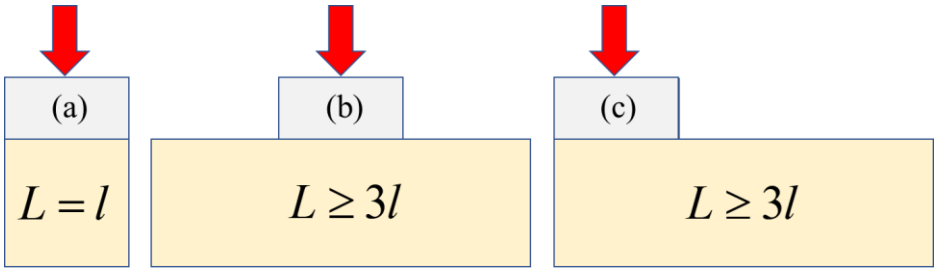

Figure 23 Three types of transverse compression: (a) Entire-surface compression (b) Intermediate-surface local compression

(c) End-surface local compression

Figure 24 shows the load-displacement curves of specimens under different loading mode. Although the bearing capacity of three loading modes is close in the initial stage, the specimen subjected to the entire-surface loading exhibits apparently highest load bearing capacity under larger deformation, which could also be explained by the load dispersed mechanism. From the above parameter studies, it can be concluded that the bearing capacity of laminated bamboo lumber under local compression can be affected by many parameters, such as the bearing shape, bearing area, loading mode. Equation (24), (25) and (29) are only suitable for intermediate-surface local compression specimens. Thus, more experimental studies should be conducted in the future to create a more universal equation.

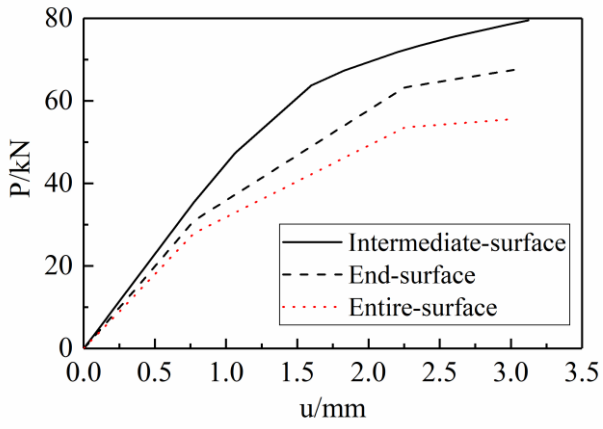

Figure 24 Load-displacemnt curves

4. Conclusions

To investigate the mechanical properties of laminated bamboo lumber under compression in the two transverse directions, 144 prismatic specimens were prepared and tested. Meanwhile, finite element analysis was conducted for revealing mechanism and parameter studies. Based on the test and FEA results, the following conclusion can be obtained:

(1) The failure patterns of specimens under entire-surface compression in the two transverse directions are similar, i.e., a 40-70 degrees shear face occurring. The failure patterns of specimens under local compression are also similar. However, there are a few distinctions between the two directions due to different

layer structure. The radial specimens under entire-surface compression exhibit apparent local buckling, while the tangential specimens under local-surface compression exhibit obvious falling off trend of side surfaces.

(2) The compressive strength and elastic modulus in the tangential direction are roughly 1.1 times higher than those in the radial direction. This may be attributed to the higher densification pressure in the tangential direction during the manufacturing process. The proportional limit strength of the specimen when compressed locally in the radial and tangential directions is 1.63 times and 1.67 times greater than when compressed entirely. The reason obtained from FEA results and theoretical analysis is that the load is dispersed throughout thickness thus effectively reduce the stress.

(3) Based on Logit model, the relationship between displacement and load of specimen under local compression in the elastic region is derived, taking into account the contact length l between steel block and specimen, as well as the height H, width b and length L of specimen.

(4) FEM results show that the bearing capacity and stress distribution of laminated bamboo lumber under local compression can be affected by many parameters, such as the bearing shape, bearing area, loading mode. Thus, more experimental studies should be conducted in the future.

Funding: This work was supported by the National Natural Science Foundation of China (No. 51878354 & 51308301); the Natural Science Foundation of Jiangsu Province (No. BK20181402 & BK20130978); Postgraduate Research &Practice Innovation Program of Jiangsu Province; 333 talent high-level project of Jiang-su Province; and Qinglan Project Fund of Jiangsu Higher Education Institutions. Any research results expressed in this paper are those of the writer(s) and do not necessarily reflect the views of the foundations.

Data Availability Statement： All data, models, and code generated or used during the study appear in the submitted article.

Acknowledgment: The writers gratefully acknowledge Ke Zhou, Xiaoyan Zheng, Shaoyun Zhu, Liqing Liu, Dunben Sun, Jing Cao, Yanjun Liu and others from Nanjing Forestry University for helping with the tests.

The authors declare that they have no conflicts of interest to this work.

Reference:

Barber, J. R. 2002. *Elasticity*. Springer.

Brandner, R. 2018. “Cross laminated timber (CLT) in compression perpendicular to plane: Testing, properties, design and recommendations for harmonizing design provisions for structural timber products.” *Eng. Struct.*, 171: 944–960. Elsevier.

Chen, G., Y. Yu, X. Li, and B. He. 2020. “Mechanical behavior of laminated bamboo lumber for structural application: an experimental investigation.” *Eur. J. Wood Wood Prod.*, 78 (1): 53–63. Springer.

Cramer, J. S. 2003. “The origins and development of the logit model.” *Logit Model. from Econ. other fields*, 2003: 1–19. Citeseer.

Dauletbek, A., H. Li, Z. Xiong, and R. Lorenzo. 2021. “A review of mechanical behavior of structural laminated bamboo lumber.” *Sustain. Struct.*, 1 (1): 000004. https://doi.org/10.54113/j.sust.2021.000004.

Dixon, P. G. 2017. “The structure and mechanical behavior of bamboo and bamboo products.” Massachusetts Institute of Technology.

Dixon, P. G., P. Ahvenainen, A. N. Aijazi, S. H. Chen, S. Lin, P. K. Augusciak, M. Borrega, K. Svedström, and L. J. Gibson. 2015. “Comparison of the structure and flexural properties of Moso, Guadua and Tre Gai bamboo.” *Constr. Build. Mater.*, 90: 11–17. Elsevier.

Dixon, P. G., S. Malek, K. E. Semple, P. K. Zhang, G. D. Smith, and L. J. Gibson. 2017. “Multiscale modelling of moso bamboo oriented strand board.” *BioResources*.

Dixon, P. G., K. E. Semple, A. Kutnar, F. A. Kamke, G. D. Smith, and L. J. Gibson. 2016. “Comparison of the flexural behavior of natural and thermo-hydro-mechanically densified Moso bamboo.” *Eur. J. Wood Wood Prod.*, 74 (5): 633–642. Springer.

Ghavami, K. 2005. “Bamboo as reinforcement in structural concrete elements.” *Cem. Concr. Compos.*, 27

(6): 637–649. Elsevier.

Hong, C., H. Li, R. Lorenzo, G. Wu, I. Corbi, O. Corbi, Z. Xiong, D. Yang, and H. Zhang. 2019. “Review on connections for original bamboo structures.” *J. Renew. Mater.*, 7 (8): 713–730. Tech Science Press.

Hong, C., H. Li, Z. Xiong, R. Lorenzo, I. Corbi, and O. Corbi. 2021a. “Experimental and numerical study on eccentric compression properties of laminated bamboo columns with a chamfered section.” *J. Build. Eng.*, 43: 102901. Elsevier.

Hong, C., H. Li, Z. Xiong, R. Lorenzo, I. Corbi, O. Corbi, D. Wei, C. Yuan, D. Yang, and H. Zhang. 2020. “Review of connections for engineered bamboo structures.” *J. Build. Eng.*, 30: 101324. Elsevier.

Hong, C., H. Li, Z. Xiong, R. Lorenzo, X. Li, and Z. Wang. 2021b. “Axial compressive behavior of laminated bamboo lumber columns with a chamfered section.” *Structures*, 678–692. Elsevier.

Jasieńko, J., T. Nowak, and D. Czepižak. 2010. “Numerical analysis of CFRP-reinforced wooden beams under bending.” *Proc. World Conf. Timber Eng. Riva del Garda ID/Paper*.

Leijten, A. J. M. 2016. “The bearing strength capacity perpendicular to grain of norway spruce–Evaluation of three structural timber design models.” *Constr. Build. Mater.*, 105: 528–535. Elsevier.

Leijten, A. J. M., A. J. M. Jorissen, and B. J. C. De Leijer. 2012. “The local bearing capacity perpendicular to grain of structural timber elements.” *Constr. Build. Mater.*, 27 (1): 54–59. Elsevier.

Li, H., G. Wu, Z. Xiong, I. Corbi, O. Corbi, X. Xiong, H. Zhang, and Z. Qiu. 2019a. “Length and orientation direction effect on static bending properties of laminated Moso bamboo.” *Eur. J. Wood Wood Prod.*, 77 (4): 547–557. Springer.

Li, H., Q. Zhang, D. Huang, and A. J. Deeks. 2013. “Compressive performance of laminated bamboo.” *Compos. Part B Eng.*, 54: 319–328. Elsevier.

Li, X., M. Ashraf, M. Subhani, P. Kremer, H. Li, and M. Anwar-Us-Saadat. 2021. “Rolling shear properties of cross-laminated timber (CLT) made from Australian Radiata Pine–An experimental study.” *Structures*,

423–432. Elsevier.

Li, Z., T. Li, C. Wang, X. He, and Y. Xiao. 2019b. “Experimental study of an unsymmetrical prefabricated hybrid steel-bamboo roof truss.” *Eng. Struct.*, 201: 109781. Elsevier.

Liu, K., D. Jayaraman, Y. Shi, K. Harries, J. Yang, W. Jin, Y. Shi, J. Wu, P. Jacome, and D. Trujillo. 2022. “‘Bamboo: A Very Sustainable Construction Material’ - 2021 International Online Seminar summary report.” *Sustain. Struct.*, 2 (1): 000015. https://doi.org/10.54113/j.sust.2022.000015.

Lv, Q., Y. Ding, and Y. Liu. 2019. “Study of the bond behaviour between basalt fibre-reinforced polymer bar/sheet and bamboo engineering materials.” *Adv. Struct. Eng.*, 22 (14): 3121–3133. SAGE Publications Sage UK: London, England.

Madsen, B., R. F. Hooley, and C. P. Hall. 1982. “A design method for bearing stresses in wood.” *Can. J. Civ. Eng.*, 9 (2): 338–349. NRC Research Press Ottawa, Canada.

Méndez Quintero, M. A., C. P. Tam Takeuchi, and H. Li. 2022. “Structural analysis of a Guadua bamboo bridge in Colombia.” *Sustain. Struct.*, 2 (2): 000020.

Mimendi, L., R. Lorenzo, and H. Li. 2022. “An innovative digital workflow to design, build and manage bamboo structures.” *Sustain. Struct.*, 2 (1): 000011. https://doi.org/10.54113/j.sust.2022.000011.

Van der Put, T. 2008. “Derivation of the bearing strength perpendicular to the grain of locally loaded timber blocks.” *Holz als Roh-und Werkst.*, 66 (6): 409–417. Springer.

Qiu, Z., and H. Fan. 2020. “Nonlinear modeling of bamboo fiber reinforced composite materials.” *Compos. Struct.*, 238: 111976. Elsevier.

Sharma, B., A. Gatóo, M. Bock, and M. Ramage. 2015. “Engineered bamboo for structural applications.” *Constr. Build. Mater.*, 81: 66–73. Elsevier.

Sinha, A., D. Way, and S. Mlasko. 2014. “Structural performance of glued laminated bamboo beams.” *J. Struct. Eng.*, 140 (1): 4013021. American Society of Civil Engineers.

Song, J., J. U. Surjadi, D. Hu, and Y. Lu. 2017. “Fatigue characterization of structural bamboo materials under flexural bending.” *Int. J. Fatigue*, 100: 126–135. Elsevier.

Su, J., H. Li, Z. Xiong, and R. Lorenzo. 2021. “Structural design and construction of an office building with laminated bamboo lumber.” *Sustain. Struct.*, 1 (2): 000010. https://doi.org/10.54113/j.sust.2021.000010.

Sun, X., M. He, F. Liang, Z. Li, L. Wu, and Y. Sun. 2021. “Experimental investigation into the mechanical properties of scrimber composite for structural applications.” *Constr. Build. Mater.*, 276: 122234. Elsevier.

Tang, G., L. Yin, Z. Li, Y. Li, and L. You. 2019. “Structural behaviors of bolted connections using laminated bamboo and steel plates.” *Structures*, 324–339. Elsevier.

Tinkler-Davies, B., and D. U. Shah. 2021. “Digital image correlation analysis of laminated bamboo under transverse compression.” *Mater. Lett.*, 283: 128883. Elsevier.

Wang, X., A. Zhou, L. Zhao, and Y. H. Chui. 2019. “Mechanical properties of wood columns with rectangular hollow cross section.” *Constr. Build. Mater.*, 214: 133–142. Elsevier.

Wang, Z., H. Li, B. Fei, M. Ashraf, Z. Xiong, R. Lorenzo, and C. Fang. 2021a. “Axial compressive performance of laminated bamboo column with aramid fiber reinforced polymer.” *Compos. Struct.*, 258: 113398. Elsevier.

Wang, Z., H. Li, D. Yang, Z. Xiong, U. Sayed, R. Lorenzo, I. Corbi, O. Corbi, and C. Hong. 2021b. “Bamboo node effect on the tensile properties of side press-laminated bamboo lumber.” *Wood Sci. Technol.*, 55 (1): 195–214. Springer.

Wei, Y., M. Zhou, K. Zhao, K. Zhao, and G. Li. 2020. “Stress–strain relationship model of glulam bamboo under axial loading.” *Adv. Compos. Lett.*, 29: 2633366X20958726. SAGE Publications Sage UK: London, England.

Yang, D., H. Li, Z. Xiong, L. Mimendi, R. Lorenzo, I. Corbi, O. Corbi, and C. Hong. 2020. “Mechanical properties of laminated bamboo under off-axis compression.” *Compos. Part A Appl. Sci. Manuf.*, 138:

106042. Elsevier.

Zhang, H., H. Li, C. Hong, Z. Xiong, and O. Corbi. 2021. “Size Effect on the Compressive Strength of Laminated Bamboo Lumber.” *J. Mater. Civ. Eng.*, 33 (7).

Zhou, K., H. Li, C. Hong, M. Ashraf, U. Sayed, R. Lorenzo, I. Corbi, O. Corbi, D. Yang, and Y. Zuo. 2021. “Mechanical properties of large-scale parallel bamboo strand lumber under local compression.” *Constr. Build. Mater.*, 271. https://doi.org/10.1016/j.conbuildmat.2020.121572.